Final Draft
of the original manuscript:

Vaidya, W.V.; Angamuthu, K.; Kocak, M.; Grube, R.; Hackius, J.:
Strength and Fatigue Resistance of Laser-MIG Hybrid Butt Welds of an Airframe Aluminium Alloy AA6013
In: Welding in the world (2006) Pergamon Press
2006 Vol. 50(11-12): 88-97

DOI: -

STRENGTH AND FATIGUE RESISTANCE OF LASER-MIG HYBRID BUTT-WELDS OF AN AIRFRAME ALUMINIUM ALLOY AA6013

W. V. Vaidya[a], K. Angamuthu[a], M. Koçak[a], R. Grube[b] and J. Hackius[c]

[a]Institute for Materials Research, Materials Mechanics,
GKSS Research Center, D-21502 Geesthacht, Germany
[b]BIAS, D-28359 Bremen, Germany
[c]AIRBUS Germany, D-28183 Bremen, Germany

Abstract: Hybrid welding is, as regards selection of welding parameters, a tolerant process. On the other hand, the weld seam and the heat affected zone may tend to be wider as in an arc process, which may be detrimental to mechanical stability. With CO_2 laser beam butt-welds as a basis for comparison, properties of butt-welds of a peak-aged airframe alloy AA6013-T6/3.2 mm, produced by Nd:YAG-MIG hybrid, are investigated. A filler wire (AA4047; AlSi12) was used for both types of welding. It is found that the hybrid process coarsened the microstructure in the fusion zone partly. Furthermore, although the weld seam and the heat affected zone were wider, mechanical properties were not at all adversely affected. Changes in hardness and tensile strength were marginal and the fatigue performance was in fact improved for the hybrid welds. These results are presented and discussed. It is concluded that the hybrid welding deserves consideration for fatigue critical applications.

Keywords: Airframe alloy, Aluminium alloy, Butt-welds, Crack initiation, Fatigue, Fatigue crack propagation, Fracture, Hardness gradient, Hybrid welds, Laser beam welds, Tensile strength

1 Introduction

Aluminium alloys are, due to their low density, a good choice for lightweight construction. When it comes to joining by fusion welding, however, a number of properties such as high thermal conductivity, high thermal expansion and high affinity for hydrogen and oxygen are not so favourable. The practical consequences are, for example, the requirement of high energy sources for welding and the susceptibility for defects such as distortion and pore formation. With the development of the high power density laser beam welding (LBW) technology and the availability of Al-alloys amenable for fusion welding, the situation has changed completely and high quality welds, nearly free from distortion and pores, can be produced. Now, LBW technology has been introduced even in metallic airframes for skin-stringer welds (T-joints) and a substantial saving in weight and production costs has been achieved by replacing riveted joints by welds [1]. Loss of alloying elements due to plasma formation, particularly of Mg which has a high vapour pressure, can be a problem. However, this can be controlled by selecting proper LBW parameters as shown by Weston et al. [2] while studying the applicability of various laser sources to butt-joints of Al-alloys. They have shown that by controlling LBW speed, which in turn controls the exposure to high temperature, the loss of alloying elements can be controlled and a good joint efficiency (in terms of tensile strength) for butt-welds can be achieved.

Recently, a hybrid process which combines the laser and the arc sources, has attracted attention. Its salient features have been surveyed and reviewed in detail [3-6]. In a nutshell, deficiencies of the individual process can be compensated through the hybrid process and synergetic effects can be achieved [3-6]. The major advantage when compared to LBW in

particular, is that the welding process becomes as tolerant as in the arc process, since related welding parameters tend to be not so critical. The weld seam, although narrower than that in the arc welding, however, tends to be wider compared to that in LBW. Nonetheless, the process has found a quick pick-up in land-based transport systems [7,8].

The purpose of the present work was to verify the possibility of hybrid welding for butt-joints of an airframe alloy. Aerospace applications imply tacitly that property changes introduced in the material by joining should be kept to a minimum. Compared to arc welding, LBW has indeed a narrower seam and heat affected zone (HAZ) in skin-stringer welds [9], which explains its applicability in airframes [1]. In the first impression, a wider seam resulting from the hybrid may mean, however, a step backwards. Interestingly, with proper parameters the situation may be made favourable. Hackius et al. [10] have shown on thin sheet (≤ 3 mm) butt-joints of Al-alloys that not only single phase (AA5754) but also precipitation hardenable multiphase (AA6082) alloys can be successfully hybrid welded nearly to pore-free quality, and the width of the hardness trough in the latter case can be kept quite comparable with that for LBW. Moreover, penalty in the loss of hardness is not so excessive. Furthermore, development at BIAS (where the present welding was undertaken) showed that the bead geometry can be controlled [11,12]. Since cracks may initiate at the bead under fatigue loading, propagate under service loading and reduce the residual strength, hybrid welding may be a way to improve the mechanical stability by avoiding undercuts and reducing the notch factor by controlling the bead geometry. On the other hand, if the bead tends to be wider and becomes more like that for the arc welding, mechanical properties may be impaired. Thus, there are pros and cons for hybrid welding, but a compromise reached may not be acceptable for a given application, say aerospace.

Whether and how far the hybrid welding can be useful has not been investigated for an airframe alloy. Therefore, the present study was undertaken as a preliminary step on AA6013. This is a fusion weldable airframe alloy having a high damage tolerance. The nominal alloy type is AlMgSiCu and can be precipitation hardened. The major hardening phase is ß-Mg_2Si; on peak ageing to T6, needle shaped ß" precipitates mainly, and rod shaped ß' and plate shaped ß lead to overaging [13]. CO_2 laser welds were used for comparison with Nd:YAG-MIG (metal inert gas) hybrid welds and a filler wire (AA4047; Al12Si) was used in both types of welding. In this work the major focus is kept on *properties* of welds, and *not* on welding itself.

2 Experimental Procedure

The nominal composition (in wt %) of the major elements was: 0.9 % Mg, 0.7 % Si, 0.9 % Cu and rest Al. The material had a nominal sheet thickness of 3.2 mm and was peak aged to T6 (190 °C - 4 h/air cooling) before welding. Plates (500X250 mm^2) were welded by using a 15 kW capacity CO_2 laser and the filler wire AA4047. For hybrid welding a 4.4 kW capacity Nd:YAG laser coupled with MIG (the feed wire AA4047 as an electrode) was used. Thereby a DC pulsed source was utilised, since the sheets were believed to be thick enough to avoid burn-through [14]. Protective inert gas shielding (He-Ar) was used in both cases. The coupon size after welding was 500X500 mm^2 with the weld in the center.

Specimens were extracted and loaded in the transverse direction to the weld. The weld seam was left unmachined for tensile and fatigue testing, but was machined for fatigue crack propagation (FCP) so as to facilitate optical crack length measurement on the specimen surface.

The microhardness profile was obtained with HV0.2 and at an indentation interval of 0.3 mm. Elongation in tensile specimens was measured by a laser extensometer over a gauge length

L_0 = 50 mm. Reduced gauge length section area was 25X50 mm^2 for the tensile specimens and 30X60 mm^2 for the fatigue specimens. For FCP testing, middle-cracked tension, M(T), specimens were extracted in the T-L direction such that FCP on the broad face occurred in the L-direction. Specimens had the dimensions: width, W = 160 mm, length, L = 480 mm and thickness, B = 3.2 mm. The initial notch, $2a_n$, was 3 mm and consisted of the central bore, Ø1 mm, and a slit of 1 mm having a width of 0.2 mm introduced by electric discharge machining on both sides of the bore. Testing was carried out on an electromechanical 50 kN (tensile), and servo-hydraulic machines of a capacity of 100 kN (fatigue) and 160 kN (FCP) in the peak-load controlled sine wave mode at f = 10 Hz (fatigue) and 25±5 Hz (FCP) in laboratory air (relative humidity ≈ 60 %). Load ratio R (= P_{min}/P_{max}) was 0.1. Since the major interest was to find out the overall nature of the FCP behaviour, raw data (without averaging) are considered here. Data were acquired manually. Crack length was measured optically at a resolution better than 0.02 mm on a surface polished to metallographic quality and marked with a measuring grid of 1 mm. On the opposite face a gauge was mounted in the load line for crack closure measurements, and load (P) versus crack opening displacement (Δv_{LL}) measurements were obtained by reducing the operating frequency to f ≈ 0.2 Hz.

3 Results and Discussion

The core question of the investigation is recalled here to provide a background, and is depicted schematically in Fig. 1. The hybrid process used utilizes two heat sources; the laser beam (Nd:YAG) combined with a conventional source, the arc (MIG). When these sources are used *alone*, the weld seam and HAZ resulting from the arc process are generally wider than those from LBW. In other words, the section, over which property changes for a given material are likely to be affected, shall be more in the arc process than in LBW, Fig. 1b. Fortunately, for the hybrid process an intermediate size for the weld seam and HAZ is to be expected. When AA6013 is peak aged by the T6 temper, it contains hardening precipitates [13] and any substantial change in the latter should affect the mechanical stability. On the welding side, however, heat has to be introduced for joining by fusion. Since the solvus temperature for precipitates is easily exceeded, not only in the fusion zone but also in HAZ, the precipitates shall be re-dissolved and the material shall soften. A wider seam and HAZ, as to be expected from the hybrid weld [10], would then mean property changes over a wider section. The question of interest is: what is the extent of these changes and can it be tolerated for a given application?

In the following, LBW refers to CO_2 laser beam weld used for comparison with the hybrid weld. Figures in colour are used to differentiate the data, particularly in case of overlapping. The beam entry side is also referred to as “top” and the opposite side as “bottom” or “back” side (for readers who may not be conversant with the terminology such as crown and root); this is an arbitrary nomenclature but is used consistently here.

3.1 Visual Observations

The welded coupons exhibited distortion (bending), had its maximum (≤ 6 mm) in the center of the coupon and did not differ for a given welding process. Furthermore, non-destructive investigations showed that both types of welds were nearly free from detectable pores within the radiographic resolution used (better than 0.1 mm). Thus, since porosity is dependent on the pick-up of gaseous impurities and the temperature during welding [15], the temperature reached in the present cases should have been comparable and the protective inert gas shielding very effective. Also, from the similarity in distortion (bending) induced, the strain and the heat flow in the hybrid welding are assumed to be of the same extent as that in LBW.

The major visual change was in the appearance of the weld, and is shown in Fig. 2. Compared to LBW which had the typical fish grating pattern on the top side and had caused occasional undercuts and spatter, the hybrid weld was smoother and shiny. The welds were otherwise clean and did not exhibit burning, blowholes or porous surface. Although the width of the seam and HAZ in the hybrid weld was larger on the top side, in the section as well as at the back side both the welds had a comparable width, with the difference that the width of the hybrid weld on the back side was not necessarily constant (see the cross-sectional macrograph in Fig. 3b to follow). Moreover, although seldom, some metal was overhanging, in the sense that occasionally frozen droplets and metallic threads were hanging on the back side and in that case the section was not so smooth as in Fig. 2e. This may be an indication of improved melting efficiency in the hybrid welding [3,16], and needs to be reduced by decreasing DC power input to avoid the overhanging. Due to the presence of weld defects or surface irregularities or both, it can be assumed in the first instance that both processes can be optimized further and the properties to be reported below, represent probably the lower bound results.

3.2 Microstructural Variations

With the beams entering from the top during the hybrid welding, it was expected that major changes in microstructure should occur at the top. Here a location having a narrow width at the back was *purposely* selected and microstructural changes were compared. The macrosections are shown in Fig. 3; the section in Fig. 3b, being non-uniform (see Fig. 2e also), was believed to be the result of a non-uniform heating and cooling. As far as the maximum width of the seam is considered, Figs. 2b, 2e and 3 show that the width in both types of welds in the cross-section is quite comparable and was successfully controlled by selecting appropriate parameters during hybrid welding [11,12].

The microstructure was investigated at a number of locations in the vertical direction (which might have experienced a thermal gradient) and compared at mirror sites in both types of welds. Some typical sites are shown in Figs. 4-6.

The only major difference was found in cells at the top, Fig. 4. Here the dendrites in the hybrid welds were marginally larger than those in LBW. Thereafter, towards the bottom, however, the fusion zone had a nearly comparable microstructure, even when the section size was narrow (Fig. 3b). The grain boundary liquation was limited to about two grains, Fig. 5, and did not show any cracking, neither within the fusion zone nor adjacent to the interface “fusion zone-base material”. The width of HAZ in the hybrid weld was slightly larger (Fig. 3), but the microstructure was comparable, Fig. 6, with the difference that the grain size was finer and more mixed in the hybrid weld. This indicates a higher heat input in the hybrid weld; in turn, the pan-caked grains (partially recrystallised initially) undergo recrystallisation within HAZ, due to which grain size changes differently. It is probably also for this reason that HAZ in the hybrid weld shows a faster etching response than that in LBW, and is seen as a colour difference in Fig. 3.

The difference in the cell size in the fusion zone and the change in grain size in HAZ do indicate higher heat input or slower cooling rate or both in the hybrid weld. However, the resulting changes are marginal.

3.3 Microhardness Gradient

Microstructural investigations indicated variations resulting from the difference in the heat input and heat flow (Figs. 4-6). This was supplemented further by microhardness measurements to find out local microstructural heterogeneities and possible critical sites.

With the weld as the center, microhardness measurements were taken along a trace across the weld in three locations (on specimens polished to metallographic quality): top, cross-section and bottom (see Fig. 2). The data are shown in Fig. 7.

The microhardness profiles were symmetrical around the weld and there was a hardness trough towards the weld; ±7 mm in LBW and ±9 mm in the hybrid weld. This is a typical trend for aluminium alloys welded in the peak aged condition [17], whereby in addition to the dissolution and overaging of precipitates in HAZ, the filler wire used (AA4047; Al-12Si) causes dilution and change in the chemical composition of the fusion zone. Except for the difference in the width of the trough, the hardness itself was comparable in the fusion zone and in HAZ in both the welds. In the base material (data outside the trough), the top and the bottom exhibited comparable curves, both in the trend and in the values. It was only in the cross-section that the hardness level was decreased, and the decrease was more in the hybrid than that in LBW. Here two critical sites were identified: the center of the fusion zone and HAZ. For the latter, the location of the critical site as identified from the decrease in hardness was 3 mm from the weld center for LBW and 4 mm for the hybrid weld, respectively (Fig. 7).

The increase in the width of the hardness trough should support that the heat input in the hybrid weld should have been higher. Fortunately, the penalty in hardness (except for that *characteristic* of the fusion zone and HAZ) was not at all different or excessive for the hybrid weld (see also [10]).

3.4 Tensile Strength

Although the penalty in the hardness value is not excessive, HAZ and the hardness trough are wider by about 30 % each in the hybrid weld than in LBW (Fig. 7). This is the region of softening and may cause loss of strength.

Here again the penalty was found to be negligible. The tensile curves are shown in Fig. 8. Certainly, when compared to the base material, both the welds exhibit a decrease in strength; the joint efficiency of the welds is about 72 % and 82% in terms of the yield strength and the ultimate tensile strength, respectively. This effect, the so-called strength undermatching, is again characteristic for welded precipitation hardenable Al-alloys. But as far as the welds are compared with each other, the hybrid process has not impaired the strength. That the weld exhibits low elongation in the standard tensile test specimen is also common, and should be attributed to the strain concentration within or adjacent to the weld [17]. Moreover, the whole deformation is concentrated to a very short length (to the first approximation, to the width of weld seam and HAZ) which, when measured over the standard gauge length (here, 50 mm) turns out to be low, although when the weld itself is ductile [17]. Nonetheless, the hybrid weld is found to possess a slightly higher elongation even in the standard specimen (Fig. 8).

Thus, although the width of trough as inferred from the microhardness gradient was higher (Fig. 7), the overall strength of the weld was not affected unfavourably through the hybrid welding (Fig. 8).

3.5 Fatigue Behaviour

Fatigue, being sensitive to defects, is a more critical evaluation parameter than the tensile strength, since surface defects may not necessarily affect the latter. The major intention was to find out the detrimental effect of defects on fatigue. Hence, the specimen surface of the welds was not processed. To recall (Section 3.1; Fig. 2), the major surface defects present

were occasional undercuts and spatter in LBW, whereas the hybrid weld was free from such defects.

For fatigue strength calculations, increase in the material thickness due to excess material in welds was neglected and the stress level was calculated using the base material plate thickness. The fatigue behaviour is shown in Fig. 9. The base material data were obtained on finely milled surface (roughness, $R_a \leq 1$ µm) and should represent the uppermost limit that can be achieved by a fusion weld.

Both the types of welds had a fatigue resistance much lower than the base material. In other words, the welding processes have a large potential for further optimisation. It was remarkable that LBW exhibited a large scatter band, and for the hybrid weld it was considerably smaller, but these data were still within the scatter band of LBW. This makes a conclusion about the ranking difficult. Assuming the lower bound curve shown as a basis for comparison, the hybrid weld is found to exhibit a better resistance to fatigue than LBW. This can be confirmed, particularly in the high cycle regime where the crack initiation phase dominates. With the stress level at 10^7 life cycles as a technical definition of run-outs (unbroken specimen) for the fatigue limit, the latter was higher by about 30 % for the hybrid weld than for LBW. This was also approximately the range, by which the fatigue resistance was improved through the hybrid weld over the entire life cycle regime.

Scatter in fatigue is nothing unusual, particularly for welds, when defects are present. The major crack initiation site for LBW was at the top whereas for the hybrid weld it was the bottom, as indicated in Fig. 10. In the former, the weld defects were present at the top (Fig. 2a). These were avoided by the hybrid welding, however, the shape of the weld at the bottom (weld root) was not optimised for the difference in the width of weld at the back (Fig. 2f) and for overhanging material. Both these defects, although occasional, appear to have induced the notch effect. It must also be pointed out here that when a LBW specimen was defect-free, its fatigue response became as good as that of the hybrid weld or even better and that too in the high life cycle regime also.

Thus, when weld defects are already present, the crack initiation phase is either absent or is short and shortens the fatigue life. How this was different in the present welds is depicted in Fig. 11. Here two stress levels are selected for comparison; near to the fast fracture in the short life cycle regime (S_{max} = 170 MPa) and near to the fatigue limit in the high life cycle regime (S_{max} = 100 MPa). In both cases, the hybrid weld had a longer life, between a factor of two to six higher than that for LBW. Due to defects, crack initiation and propagation in LBW occurred at a number of sites. In the hybrid weld crack initiation also occurred at many places, but, apparently, some of them turned out to be non-propagating cracks and only one became the major site leading to fracture. The former is seen as wave line and the latter as the typical thumbnail shape. Furthermore, the area of crack propagation was larger in the hybrid weld (Fig. 11c-d). Note also the changeover in the crack initiation site from top to bottom in the hybrid weld (see Fig. 10 also).

Thus, the hybrid process may offer a way to improve the fatigue performance by avoiding surface defects.

3.6 Fatigue Crack Propagation

When defects are present and the crack initiation phase is absent or is short, the fatigue life shall be dominated by the crack propagation phase. The FCP behaviour of the present welds is shown in Figs. 12-13 for the notch location in the mid-fusion zone and in HAZ. The base material data were used for comparison. So as to obtain FCP data over a wide range, two

starting ΔK levels were used: about 3 MPa√m and 8 MPa√m. In Figs. 12-13, the symbol for a batch is kept the same but the colour is varied to differentiate between the starting ΔK levels. For example, square symbols but two colours, green and blue, are used for the base material data and for the batch designation, BM.

During propagation, the crack was found to remain confined to that zone where the notch was initially located and excessive crack deviation or deflection was not observed. Although there had been microstructural differences between the fusion zone (cast microstructure) and the base material (wrought microstructure), FCP response was nearly comparable over a wide ΔK range ($\leq$ 18 MPa√m). Thereafter, the weld exhibited an inferior FCP behaviour, Fig. 12. A difference in FCP depending on the welding process was, however, not present. FCP in HAZ also exhibited a similar trend, with the difference that the resistance to FCP was slightly improved compared to that of the base material, Fig. 13. Welding generally induces residual stresses, which may modify the loading spectrum and become detrimental to FCP. An AlMgSiCu-alloy (AA6056-T6/3.2 mm), laser beam welded under comparable conditions, is found to contain peak tensile residual stresses of about 180 MPa [18]. The present FCP data show, however, that even if such tensile residual stresses may have been present, the related effect on FCP is not at all pronounced and if any, the effect is marginal.

Thus, softening in HAZ although present (Fig. 7), was certainly not detrimental to FCP. Recalling that HAZ microstructure contained mixed grain sizes and shapes (Fig. 6), it is tempting to suggest that this can be a way to improve the FCP behaviour.

In the present context, the hybrid weld did not impair the resistance to FCP, neither in the fusion zone nor in HAZ.

4 Conclusions

1. Butt-welds of 3.2 mm thick AA6013 sheets, welded in the T6 (peak-aged) condition by using the CO_2 laser beam and the Nd:YAG laser-MIG hybrid process, were found to be sound and free from pores. In contrast to the CO_2 laser beam weld, surface defects such as undercuts and spatter were absent in the hybrid weld.
2. Microstructural investigations indicated variations resulting from the difference in the heat input and heat flow. In the hybrid weld the dendrites were coarser and grain size in the heat affected zone was mixed. However, such differences were marginal.
3. Both the types of welds exhibited characteristic strength undermatching. The hardness trough was relatively wider in the hybrid weld than that in the CO_2 laser beam weld. Nonetheless, hardness and tensile strength were comparable in both welds.
4. Fatigue resistance was improved in the hybrid weld, particularly in the high life cycle regime. This is attributed to the avoidance of surface defects.
5. The hybrid weld did not impair the resistance to fatigue crack propagation in the mid-regime.
6. Since a number of properties are not affected adversely, the hybrid welding deserves consideration for fatigue critical applications in particular.

Acknowledgement: The present work was supported by internal funding at GKSS, BIAS and AIRBUS. We gratefully acknowledge this financial support. Dr. K. Angamuthu, now returned to Crescent Engineering College, Vandalur, Chennai, India, is grateful for the opportunity to work at GKSS.

References

[1] W. Zink, Integral solutions for fuselage shells, in *Proceedings of the 19th European Conference on Materials for Aerospace Applications, Dec. 6-8, 2000, Munich (Germany), Advanced Aerospace Materials*, M. Peters and W. A. Kaysser, eds., *DGLR Report 2001-02*, Deutsche Gesellschaft für Luft- und Raumfahrt-Lilienthal-Oberth e. V., Bonn, Germany, 2000, pp. 25-32.

[2] J. Weston, J. W. Yoon and E. R. Wallach, Laser welding of aluminium alloys using different laser sources, *web article* (html version, http://happyinmotion.com/jez, found through Google Scholar; *Proceedings of the 6th International Conference on Welding and Melting by Electron & Laser Beams, Toulon, France, 15-19 June, 1998*).

[3] J. Tusek and M. Suban, Hybrid welding with arc and laser beam, *Science and Technology of Welding and Joining*, 1999, Vol. 4, pp. 308-311.

[4] U. Dilthey and A. Wieschemann, Prospects by combining and coupling laser beam and arc welding processes, *Welding in the World*, 2000, Vol. 44, pp. 37-46.

[5] R. W. Messler, Jr., What is next for hybrid welding, *Welding Journal*, 2004, Vol. 83, (March), pp. 30-34.

[6] C. Bagger and F. O. Olsen, Review of laser hybrid welding, *Journal of Laser Applications*, 2005, Vol. 17, pp. 2-14.

[7] L. Bertling and H. Harlfinger, Innovative Fügeverfahren zur Herstellung von Al-Leichtbaustrukturen in Schienenfahrzeug, in German, (Innovative joining techniques for creating light-weight aluminium structures in railway vehicle production), *Materialwissenschaft und Werkstofftechnik*, 1999, Vol. 30, pp. 290-299.

[8] T. Graf and H. Staufer, Laser-Hybrid welding drives VW improvements, *Welding Journal*, 2003, Vol. 82, (Jan.), pp. 44-48.

[9] G. Neye and P. Heider, Laser beam welding of modern Al-alloys for aircraft industry, in *Proceedings of ECLAT'94, 5th European Conference on Laser Treatment of Materials*, Sept. 26-27, 1994, Bremen-Vogelsack, Germany, DVS-Berichte Band 163, Deutsche Verlag für Schweißtechnik DVS-Verlag, Düsseldorf, Germany, 1994, pp. 108-117.

[10] J. Hackius, B. Brenner, B. Winderlich, J. Standfuß and E. Beyer, Laserhybrid-schweißen von Aluminiumlegierungen, in German, (Laser hybrid welding of aluminium alloys), *LaserOpto*, 2001, Vol. 33, pp. 49-55.

[11] C. Walz, T. Seefeld and G. Sepold, Nahtgeometrie und Prozessstabilität beim Laser-MIG-Schweißen, in German, (Seam geometry and process stability during laser-MIG welding), *LaserOpto*, 2001, Vol. 33, pp. 64-67.

[12] M. El Rayes, C. Walz and G. Sepold, The influence of various hybrid welding parameters on bead geometry, *Welding Journal*, 2004, Vol. 83, (May), pp. 147-S-153-S.

[13] B. Heinz and B. Skrotzki, Characterization of a friction-stir-welded aluminium alloy 6013, *Metallurgical and Materials Transactions B*, 2002, Vol. 33B, pp. 489-498.

[14] T. Ueyama, H. Hong, I. Yazawa, M. Hirami, T. Kihara, K. Nakata and M. Ushio, Aluminium alloy sheet welding by the laser AC pulsed MIG hybrid process, *Welding International*, 2004, Vol. 18, pp. 345-350.

[15] M. Mazur, Porosity in aluminium welds, *Welding International*, 1992, Vol. 6, pp. 929-931.

[16] B. Hu and G. den Ouden, Synergetic effects of laser hybrid/arc welding, *Science and Technology of Welding and Joining*, 2005, Vol. 10, pp. 427-431.

[17] W. V. Vaidya, M. Koçak, E. Seib, H. Assler and J. Hackius, Mechanical behavior of laser beam and friction stir welded aluminium alloys for airframes, *Welding in the World*, 2004, Vol. 48, (special issue, July), pp. 261-273.

[18] P. Staron, W. V. Vaidya, M. Koçak, J. Homeyer and J. Hackius, Residual stresses in laser beam welded butt joints of the airframe aluminium alloy AA6056, accepted for publication in the *Proceedings of the 7th European Conference on Residual Stresses*

(ECRS 7), 13-15 Sept., 2006, Berlin, Germany (to be published in *Materials Science Forum*).

Figure Captions

Fig. 1: Schematic representation of the hybrid process used after BIAS and a comparison of the weld seam and the heat affected zone in terms of the hardness profile when the laser beam and the arc source are used *alone*. Schematics in b) which is based on the data by Neye and Heider in ref. [9] on a welded T-joint, is exaggerated and is not to scale.

Fig. 2: Surface appearance of the CO_2 laser beam weld (upper macrographs; a-c) and the hybrid weld (lower macrographs; d-e) in a 3.2 mm thick AA6013 sheet butt-welded in T6. The surface was cleaned, the cross-section was polished and lightly etched. Local height differences in the weld are seen as surface irregularities.

Fig. 3: A comparison of the butt-weld in the cross-section, a) CO_2 laser beam weld and b) hybrid weld (section extracted *purposely* from an unusually small width on the back; see also Fig. 2e) in a 3.2 mm thick AA6013 sheet welded in T6. The frames mark the approximate areas shown in the following Figs. 4-6. Colour difference on either side of the weld is resulting from the difference in etching response in the heat affected zone.

Fig. 4: Difference in the dendritic structure in the upper section of the fusion zone in a) CO_2 laser beam weld and b) hybrid weld in a 3.2 mm thick AA6013 sheet butt-welded in T6 (see the frame in Fig. 3 for approximate location).

Fig. 5: Grain boundary liquation (seen as a thickening of grain boundaries near to the interface) in a) CO_2 laser beam weld and b) hybrid weld in a 3.2 mm thick AA6013 sheet butt-welded in T6 (see the frame in Fig. 3 for approximate location).

Fig. 6: Changeover in the microstructure on-going from the base material to the heat affected area (from left to right) in a) CO_2 laser beam weld and b) hybrid weld in a 3.2 mm thick AA6013 sheet butt-welded in T6 (see the frame in Fig. 3 for approximate location).

Fig. 7: Microhardness gradient in a) CO_2 laser beam weld and b) hybrid weld in a 3.2 mm thick AA6013 sheet butt-welded in T6. Insets indicate the locations used for microhardness measurements. The notch location in the heat affected zone (used for fatigue crack propagation tests) is shown in relation to the microhardness dip.

Fig. 8: Tensile curves (gauge length L_0 = 50 mm) and the fracture location in the CO_2 laser beam weld and the hybrid weld in a 3.2 mm thick AA6013 sheet butt-welded in T6. The fracture location is restricted to the weld.

Fig. 9: Comparative fatigue behaviour of the CO_2 laser beam weld and the hybrid weld in a 3.2 mm thick AA6013 sheet butt-welded in T6. Run-outs (i.e., unbroken specimens) are indicated by arrows.

Fig. 10: Dependence of the fatigue crack initiation site in a) CO_2 laser beam weld and b) hybrid weld in a 3.2 mm thick AA6013 sheet butt-welded in T6, tested at R = 0.1 and f = 10 Hz.

Fig. 11: Difference in the fatigue crack initiation site and the life cycles at a given stress level S_{max} in the CO_2 laser beam weld, a)-b), and the hybrid weld, c)-d), in a 3.2 mm thick AA6013 sheet butt-welded in T6, tested at R = 0.1 and f = 10 Hz (fracture halves flapped open; the arrows indicate the crack initiation sites).

Fig. 12: Fatigue crack propagation behaviour in the fusion zone of the CO_2 laser beam weld and the hybrid weld in a 3.2 mm thick AA6013 sheet butt-welded in T6. The base material data are also shown for comparison. The notch location is shown in the insets.

Fig. 13: Fatigue crack propagation behaviour in the heat affected zone of the CO_2 laser beam weld and the hybrid weld in a 3.2 mm thick AA6013 sheet butt-welded in T6. The base material data are also shown for comparison. The notch location is shown in the insets.

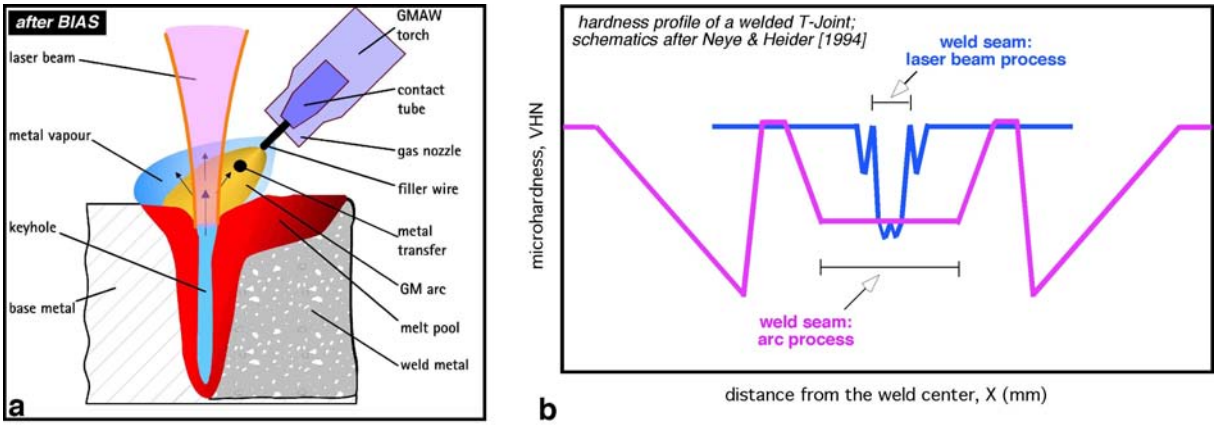

Fig. 1: Schematic representation of the hybrid process used after BIAS and a comparison of the weld seam and the heat affected zone in terms of the hardness profile when the laser beam and the arc source are used alone. Schematics in b) which is based on the data by Neye and Heider in ref. [9] on a welded T-joint, is exaggerated and is not to scale.

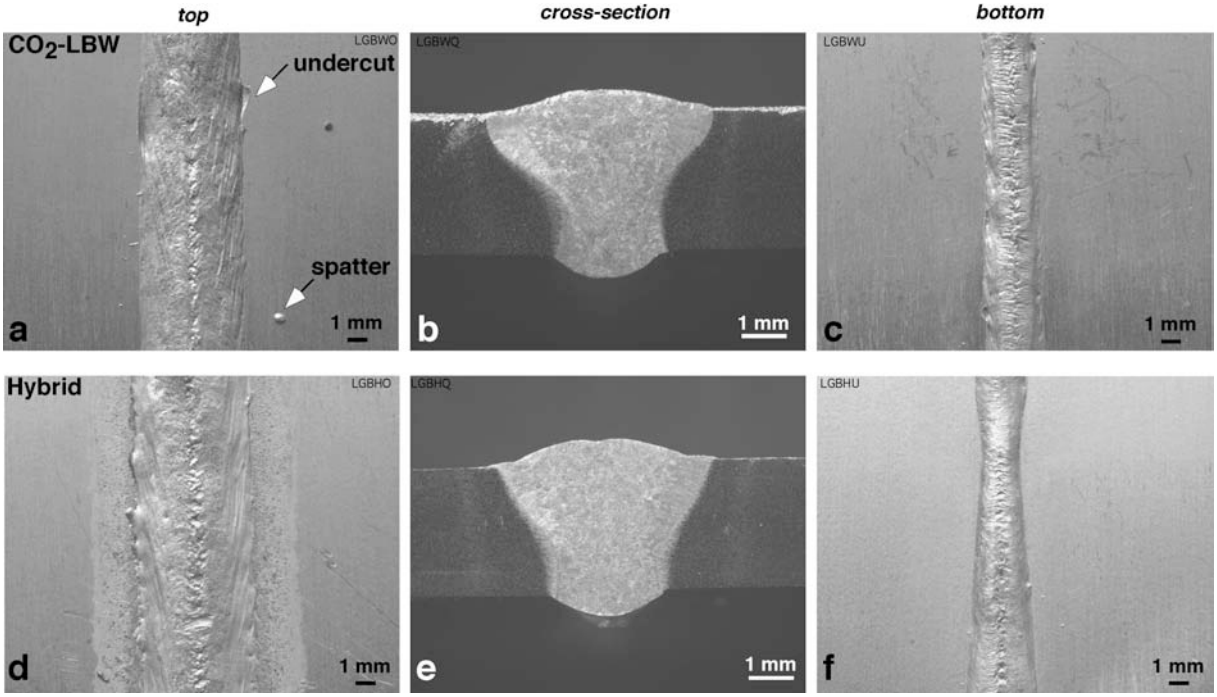

Fig. 2: Surface appearance of the CO_2 laser beam weld (upper macrographs; a-c) and the hybrid weld (lower macrographs; d-e) in a 3.2 mm thick AA6013 sheet butt-welded in T6. The surface was cleaned, the cross-section was polished and lightly etched. Local height differences in the weld are seen as surface irregularities.

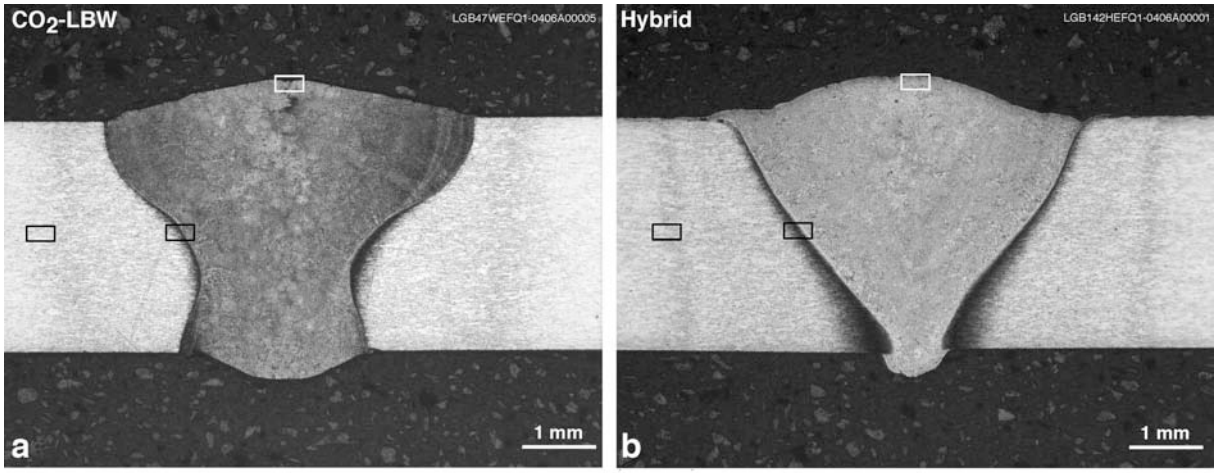

Fig. 3: A comparison of the butt-weld in the cross-section, a) CO_2 laser beam weld and b) hybrid weld (section extracted purposely from an unusually small width on the back; see also Fig. 2e) in a 3.2 mm thick AA6013 sheet welded in T6. The frames mark the approximate areas shown in the following Figs. 4-6. Colour difference on either side of the weld is resulting from the difference in etching response in the heat affected zone.

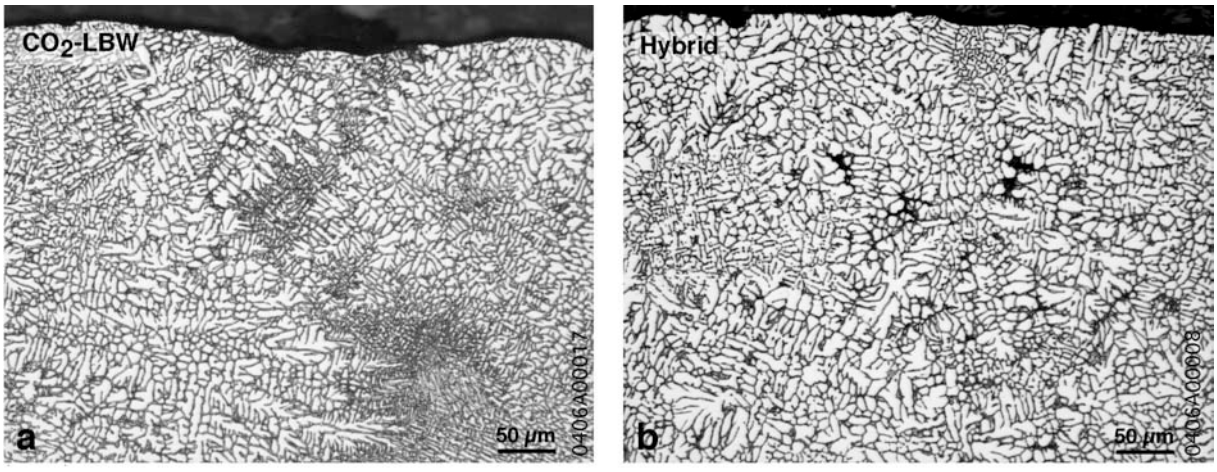

Fig. 4: Difference in the dendritic structure in the upper section of the fusion zone in a) CO_2 laser beam weld and b) hybrid weld in a 3.2 mm thick AA6013 sheet butt-welded in T6 (see the frame in Fig. 3 for approximate location).

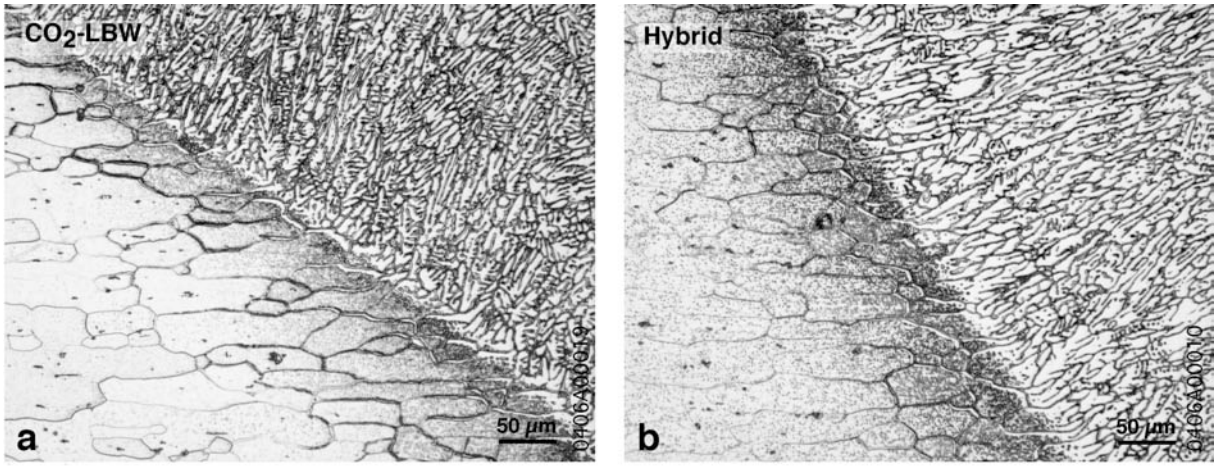

Fig. 5: Grain boundary liquation (seen as a thickening of grain boundaries near to the interface) in a) CO_2 laser beam weld and b) hybrid weld in a 3.2 mm thick AA6013 sheet butt-welded in T6 (see the frame in Fig. 3 for approximate location).

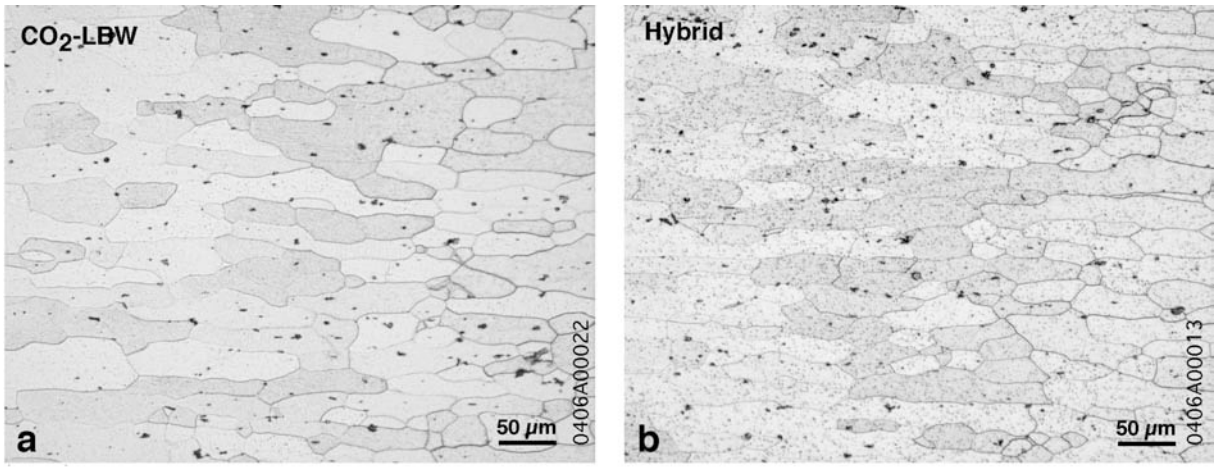

Fig. 6: Changeover in the microstructure on-going from the base material to the heat affected area (from left to right) in a) CO_2 laser beam weld and b) hybrid weld in a 3.2 mm thick AA6013 sheet butt-welded in T6 (see the frame in Fig. 3 for approximate location).

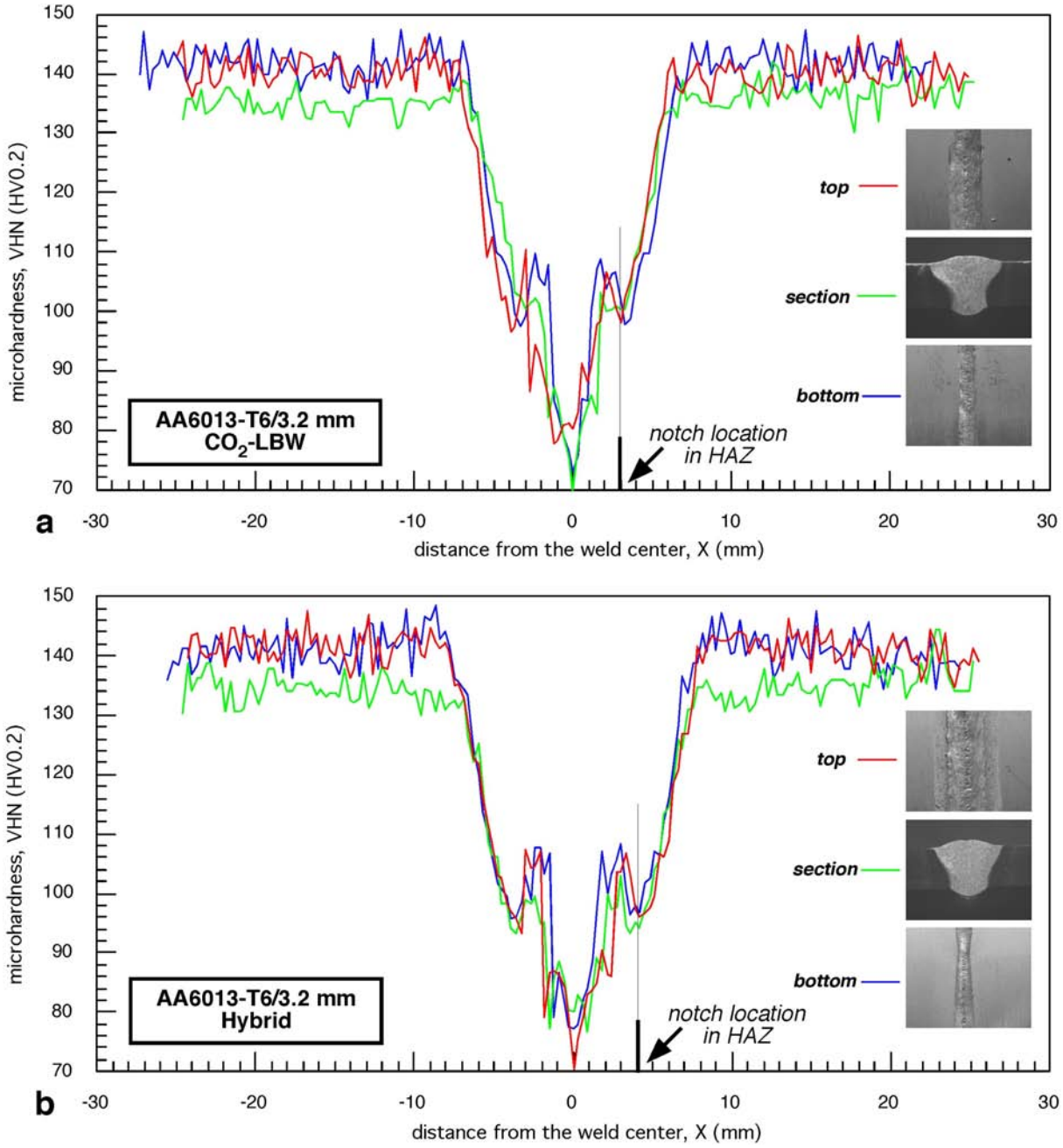

Fig. 7: Microhardness gradient in a) CO_2 laser beam weld and b) hybrid weld in a 3.2 mm thick AA6013 sheet butt-welded in T6. Insets indicate the locations used for microhardness measurements. The notch location in the heat affected zone (used for fatigue crack propagation tests) is shown in relation to the microhardness dip.

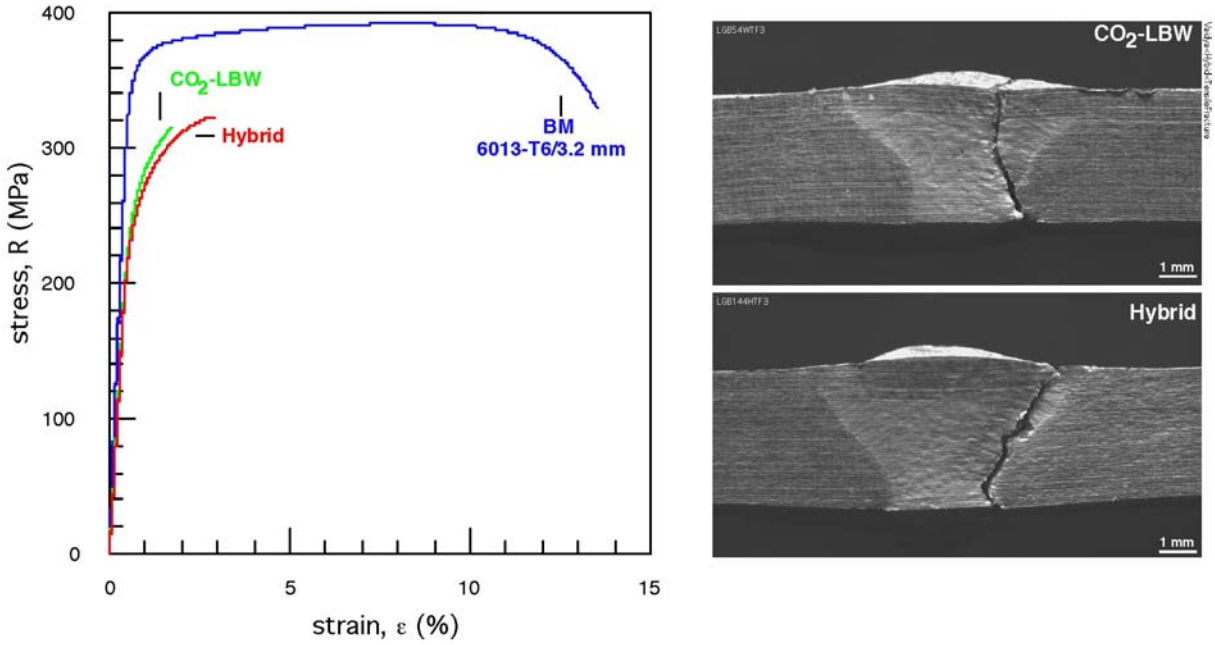

Fig. 8: Tensile curves (gauge length L_0 = 50 mm) and the fracture location in the CO_2 laser beam weld and the hybrid weld in a 3.2 mm thick AA6013 sheet butt-welded in T6. The fracture location is restricted to the weld.

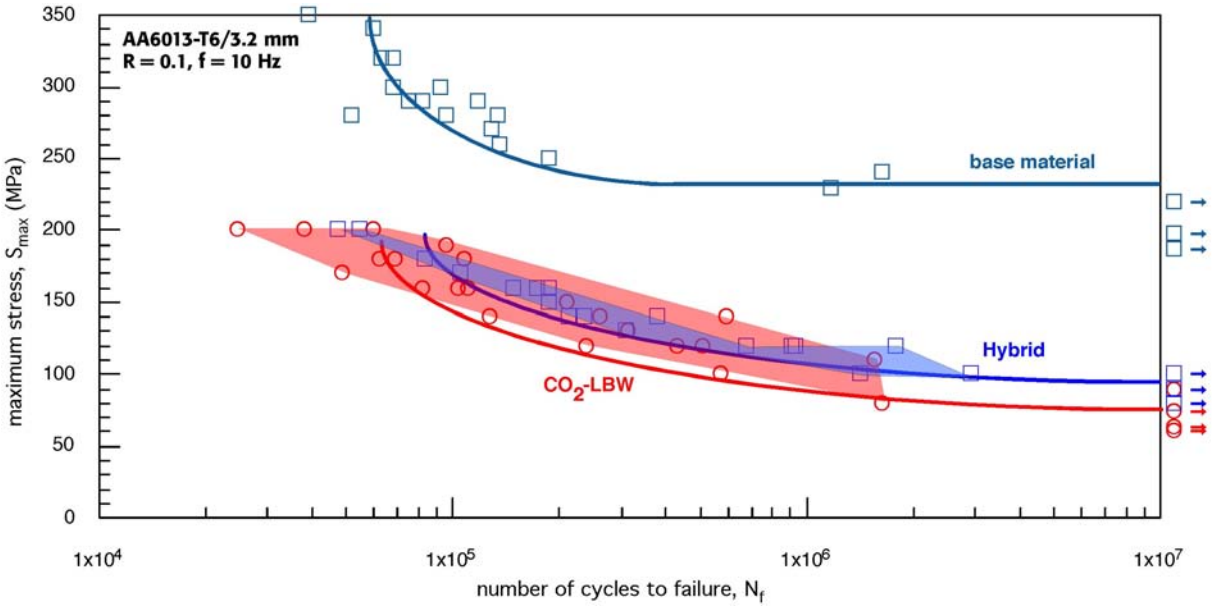

Fig. 9: Comparative fatigue behaviour of the CO_2 laser beam weld and the hybrid weld in a 3.2 mm thick AA6013 sheet butt-welded in T6. Run-outs (i.e., unbroken specimens) are indicated by arrows.

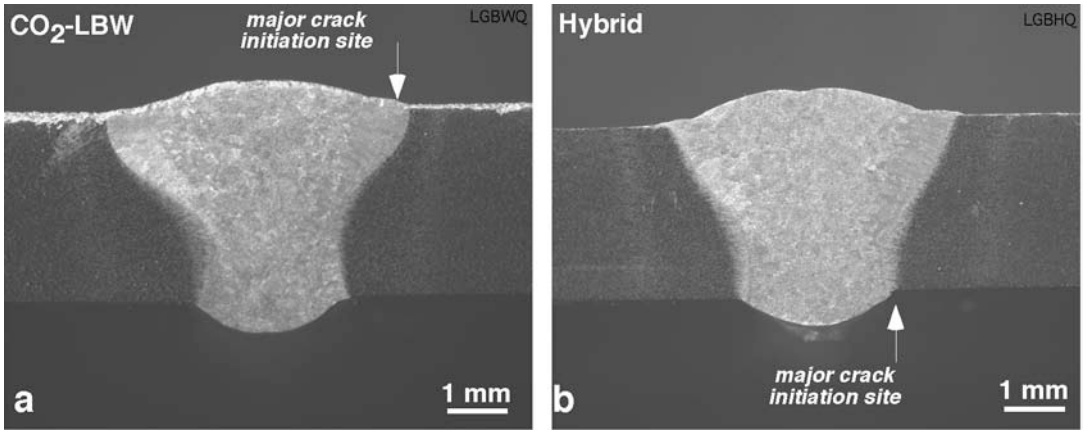

Fig. 10: Dependence of the fatigue crack initiation site in a) CO_2 laser beam weld and b) hybrid weld in a 3.2 mm thick AA6013 sheet butt-welded in T6, tested at R = 0.1 and f = 10 Hz.

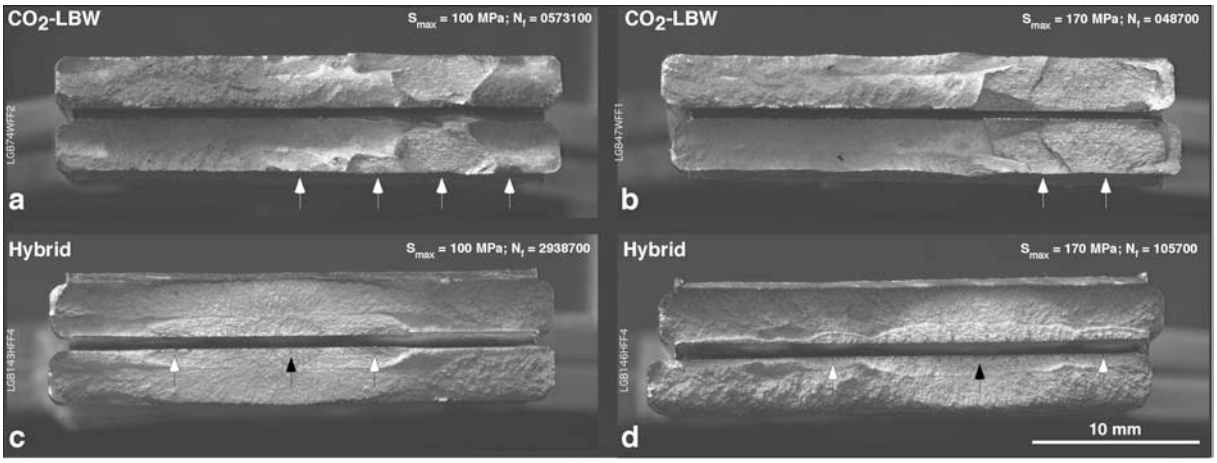

Fig. 11: Difference in the fatigue crack initiation site and the life cycles at a given stress level S_{max} in the CO_2 laser beam weld, a)-b), and the hybrid weld, c)-d), in a 3.2 mm thick AA6013 sheet butt-welded in T6, tested at R = 0.1 and f = 10 Hz (fracture halves flapped open; the arrows indicate the crack initiation sites).

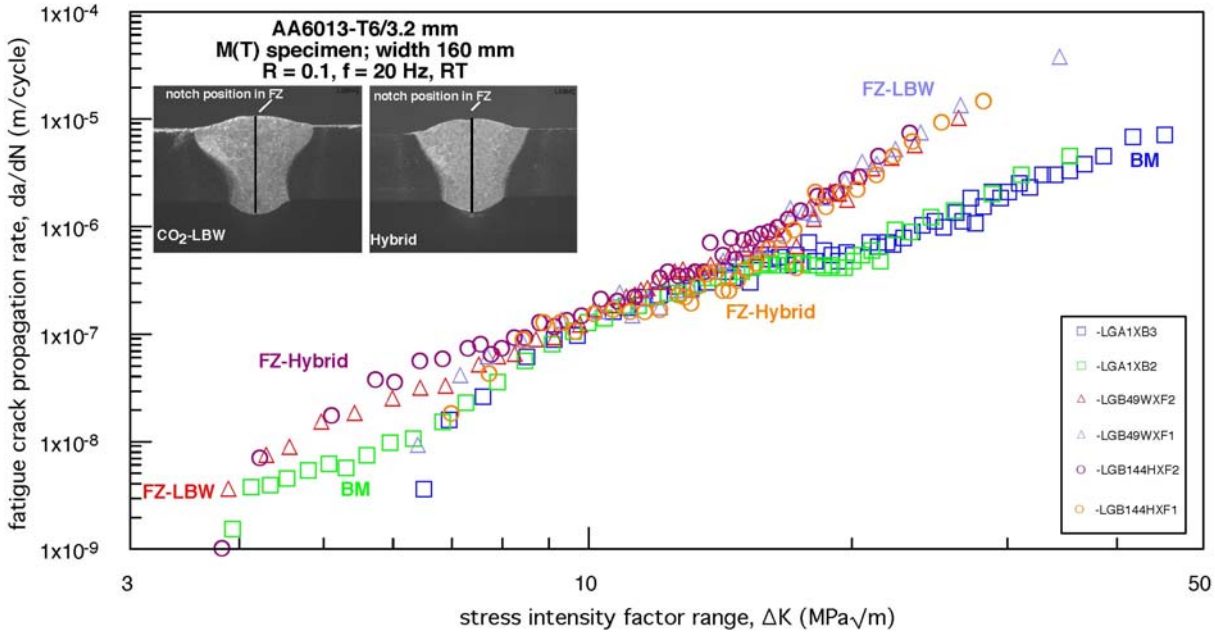

Fig. 12: Fatigue crack propagation behaviour in the fusion zone of the CO_2 laser beam weld and the hybrid weld in a 3.2 mm thick AA6013 sheet butt-welded in T6. The base material data are also shown for comparison. The notch location is shown in the insets.

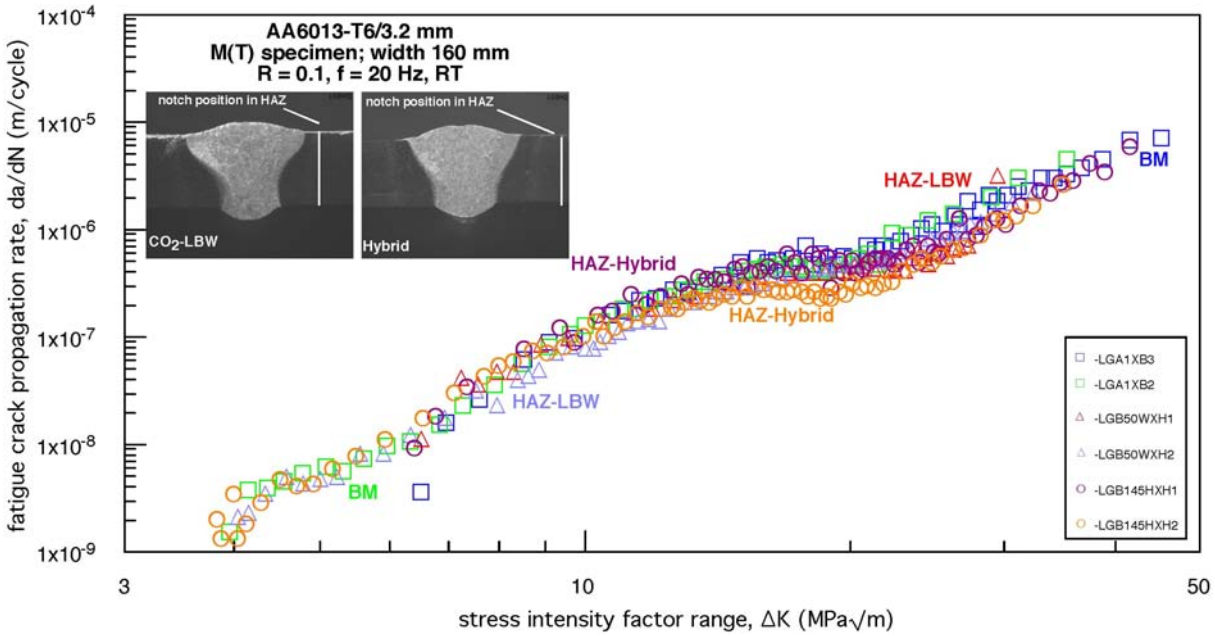

Fig. 13: Fatigue crack propagation behaviour in the heat affected zone of the CO_2 laser beam weld and the hybrid weld in a 3.2 mm thick AA6013 sheet butt-welded in T6. The base material data are also shown for comparison. The notch location is shown in the insets.